Chapter 5

A simple theoretical model for the Undulating Twist Grain Boundary phase

5.1 Introduction
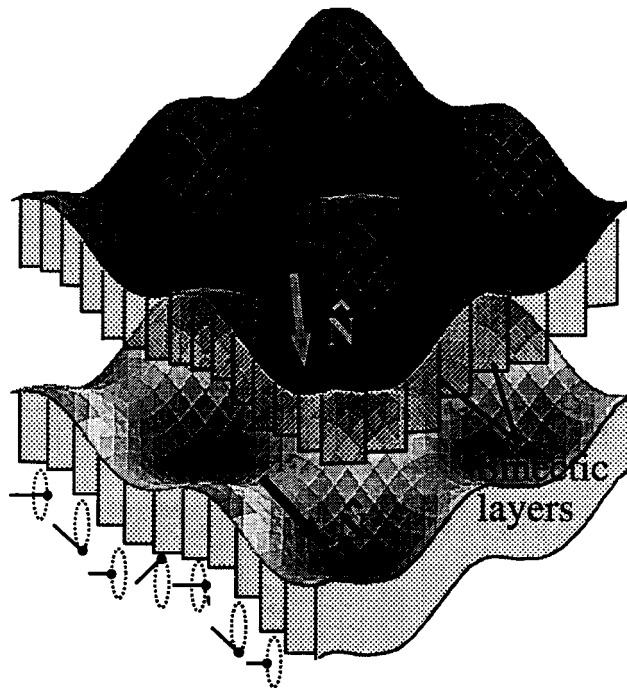

Figure 5.1: A schematic representation of the proposed structure for the $UTGB_{C^*}$ phase. The shaded area represents the two-dimensionally undulated grain boundary region. The smectic layer normals (large arrows) rotates from block to block. Within each block the Frank-director precesses along the layer normal direction as represented by the nails.

In the previous chapter we discussed the experimental observation of the new Undulating Twist Grain Boundary phase which has a smectic-C*-like structure within the blocks ($UTGB_{C*}$). Unlike the TGB_A or the TGB_C phases this phase has a three-dimensionally modulated structure. Apart from the usual TGB pitch, the grain boundaries have two-dimensional undulations along directions which are orthogonal to the TGB twist axis. Moreover, within the smectic blocks the director has a helical configuration. Thus the overall structure is far more complicated than those of the other two known TGB liquid crystals. This makes any detailed theoretical analysis quite difficult. We have developed a highly simplified model which can account for the occurrence of the various TGB phases. Before going into the details of this model, we first give a brief review of the model developed by Renn and Lubensky for the TGB_A phase, which is the simplest of the TGB phases.

5.1.1 The **Renn-Lubensky** model

The TGB_A phase was successfully predicted by Renn and Lubensky [8] and discovered by Goodby et al. The relevant structure consists of a regular twisted arrangement of almost perfect smectic-A blocks separated by grain boundaries (Fig. 5.2). Each grain boundary is made up of an array of screw dislocations. The Frank-director has a twist deformation across each grain boundary. This structure is stable over the uniform smectic-A structure when the chiral energy gained due to the twist exceeds the energy cost for generating screw dislocations. These energies are calculated as follows.

The Frank elastic free energy due to distortions in the director field of a nematic is given by

$$F_N = \frac{1}{2} \int d^3x \left[K_{11}(\boldsymbol{\nabla} \cdot \hat{\mathbf{n}})^2 + K_{22}(\hat{\mathbf{n}} \cdot \boldsymbol{\nabla} \times \hat{\mathbf{n}})^2 + K_{33}(\hat{\mathbf{n}} \times \boldsymbol{\nabla} \times \hat{\mathbf{n}})^2 \right] , \qquad (5.1)$$

where the constants K_{11}, K_{22} and K_{33} are the elastic constants corresponding to the splay, twist and bend distortions in the director field, respectively. In the case
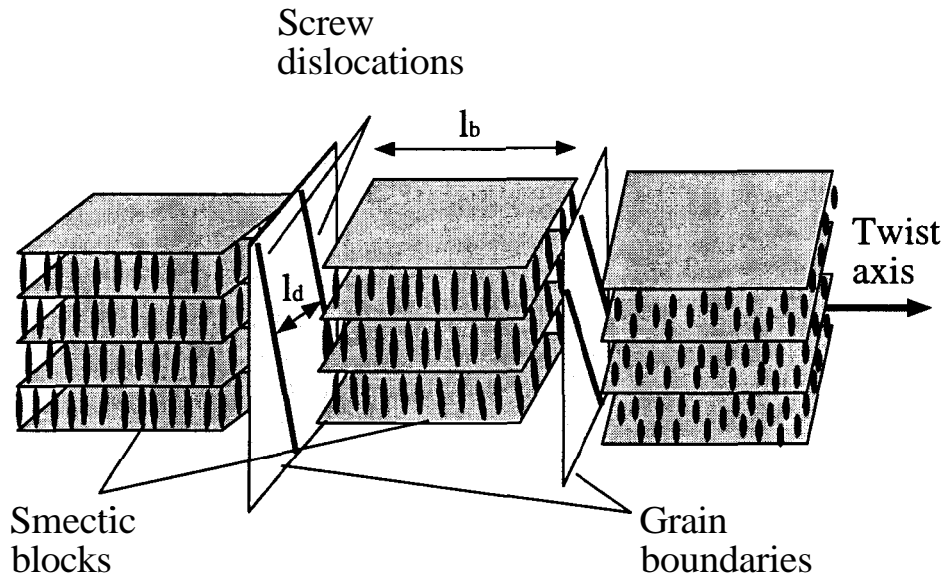
Screw
dislocations

l_b

Twist
axis

l_d

Smectic
blocks

Grain
boundaries

Figure 5.2: A schematic diagram of the *TGB*, structure. The pitch of the structure is determined by the distance l_d between the screw dislocations within a grain boundary, the distance l_b between grain boundaries and the smectic layer spacing d. In TGB_A, l_d and l_b are usually of the order of a few hundred angstroms.

of cholesterics, however, an additional chiral term is allowed in the free energy expression which is written as

$$F_{N^*} \;=\; F_N + K_{22}q_o \int d^3x (\hat{\mathbf{n}} \cdot \boldsymbol{\nabla} \times \hat{\mathbf{n}}) \,, \tag{5.2}$$

where $K_{22}q_o = \mathbf{A}$ is referred to as the chiral strength of the medium. Minimising the cholesteric free energy, **Eq.** 5.2, with respect to variations in $\hat{\mathbf{n}}$ gives a stable configuration

$$\hat{\mathbf{n}}_o(z) = [\cos(q_o z), \, \sin(q_o z), \, 0] \,, \tag{5.3}$$

which describes the cholesteric structure with the pitch defined as $p_{N^*} = 2\pi/q_o$. Both **A** and K_{22} are assumed to be independent of temperature.

The covariant form of the Landau-Ginzburg free energy expression extended to describe the nematic–Smectic-A (NA) transition by de Gennes is

$$F_S = \int d^3x \left\{ r|\psi|^2 + \left[(C_\parallel - C_\perp)n_j n_k + C_\perp \delta_{jk} \right] [(\boldsymbol{\nabla} - iq_A \hat{\mathbf{n}})_j \psi (\boldsymbol{\nabla} + iq_A \hat{\mathbf{n}})_k \psi^*] + \frac{g}{2}|\psi|^4 \right\},$$

$$\tag{5.4}$$

where r $\propto$ (T $- T_{NA}$) and $q_A = 2\pi/d$ (d is the smectic layer spacing).

In order to simplify the analysis, it is assumed that the molecules are confined to a plane orthogonal to the cholesteric twist axis. Thus, the director can be described by an angle β as

$$\hat{\mathbf{n}}(z) = [\cos\beta(z), \sin\beta(z), 0].$$ (5.5)

With this assumption we can write, $(\hat{\mathbf{n}} \cdot \nabla \times \hat{\mathbf{n}}) = \nabla_z\beta$. Further, it is assumed that $C_\| = C_\perp = C$ and $K_{11} = K_{33} = K$. With these approximations the total free energy expression, $F = F_{N^*} + F_S$, reduces to the form

$$
\begin{aligned}
F &= \int d^3x \left\{ r|\psi|^2 + C|(\nabla - iq_A\hat{\mathbf{n}})\psi|^2 + \frac{g}{2}|\psi|^4 \right\} \\
&+ \frac{1}{2}\int d^3x \left\{ K(\nabla_\perp\beta)^2 + K_{22}(\nabla_z\beta - q_o)^2 - K_{22}q_o^2 \right\}.
\end{aligned}
$$ (5.6)

In the cholesteric phase, $\psi = 0$ and $\nabla_z\beta = q_o$ so that the free energy density in this phase is $-\frac{1}{2}K_{22}q_o^2 = -\Lambda^2/K_{22}$. In the uniform smectic-A phase, $(\nabla - iq_A\hat{\mathbf{n}})\psi = 0$ and $|\psi|^2 = -r/g$ so that its free energy density is $-\frac{1}{2}r^2/g$. Equating the free energy densities in the two phases gives the thermodynamic critical chiral strength as

$$\Lambda_c = \left(\frac{K_{22}r^2}{g}\right)^{1/2}.$$ (5.7)

Thus, Λ_c is the analogue of the critical magnetic field H_c for the superconductor to the normal metal transition in a type-I superconductor. Like in superconductors it is possible to define two important lengths from the free energy expression (Eq. 5.6), namely, the correlation length for the smectic order parameter

$$\xi = (C/|r|)^{1/2}$$ (5.8)

and the twist penetration depth

$$\lambda_2 = \frac{1}{q_A}\left[\frac{K_{22}\,g}{2C|r|}\right]^{1/2}.$$ (5.9)

The analogue of the Ginzburg parameter is thus the ratio

$$\kappa_2 = \frac{\lambda_2}{\xi} = \frac{1}{Cq_A}\left[\frac{gK_{22}}{2}\right]^{1/2}$$ (5.10)

As already discussed in the previous chapter, smectics, like superconductors, can be classified as type-I or type-I1 depending on the value of κ_2. If the smectic is of type-II one would expect a state where twist deformations penetrate the smectic in the form of screw dislocations. Thus, there should be a liquid crystalline analogue of the Abrikosov phase exhibited by type-I1 superconductors. In the case of a superconductor the interactions between the magnetic flux tubes are isotropic and repulsive. Therefore, the minimum energy configuration is a triangular lattice of parallel flux tubes. In the case of smectics, however, such a simple configuration with parallel screw dislocations will cause the gradient of the layer displacement field to diverge with system size (see Sec. 4.1) and hence cannot form a thermodynamically stable state.

Renn and Lubensky realised that this problem can be overcome if the dislocations are confined to a parallel set of planes. Adjacent planes are rotated with respect to each other. Each grain boundary contains a linear array of parallel screw dislocations and is referred to as a Twist Grain Boundary (Figs. **5.2** & **5.3**). Such an array of screw dislocations causes the smectic layer normal to rotate by an angle $\Delta\beta$ across the grain boundary. This in turn results in a twist deformation in the Frank-director, thereby gaining chiral energy as given by Eq. 5.2. This phase is referred to as the Twist Grain Boundary (TGB) phase. The average twist in the structure is determined by the distance l_d between dislocations within the grain boundaries, the distance l_b between adjacent grain boundaries and the smectic layer spacing d. The angle between the smectic layer normals in adjacent blocks is (Fig. **5.3**)

$$\Delta\beta = 2\tan^{-1}\left(\frac{d}{2l_d}\right) \sim \frac{d}{l_d}, \tag{5.11}$$

where it is assumed that d $\ll l_d$ in writing the last part. If l_b is the distance between the grain boundaries, the average rate of change in β is

$$\langle q_{tgb}\rangle = \frac{1}{l_b}\int_0^{l_b} dz\nabla_z\beta(z) = \frac{\Delta\beta}{l_b} = \frac{d}{l_d l_b}. \tag{5.12}$$
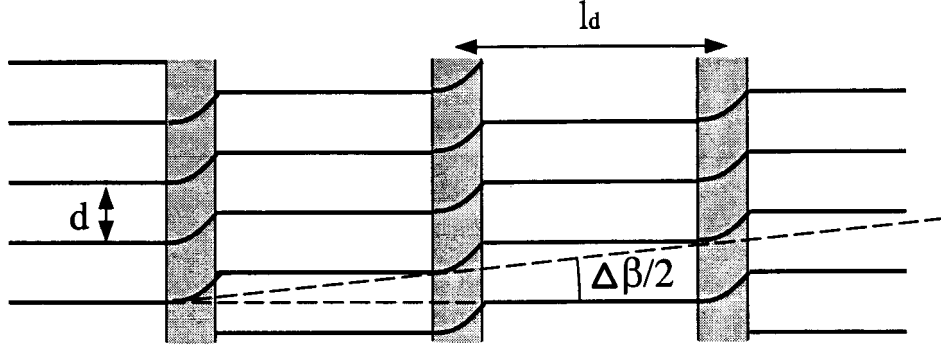
Figure **5.3:** Schematic drawing of a twist grain boundary. The screw dislocation cores are marked by the shaded regions. The smectic layers increase in height by $\frac{1}{2}d$ on taking a half (π) loop around each dislocation. The average slope of the smectic layers with respect to a plane orthogonal to the dislocations is $\frac{1}{2}d/l_d$ on oneside of the grain boundary and $-\frac{1}{2}d/l_d$ on the other side.

Using this expression for $\langle q_{tgb} \rangle = ((\text{ii} \cdot \nabla \times \text{ii}))$ in the Frank free energy Eq. **5.2** gives the average gain in chiral energy due to the twist distortion as

$$f_{twist} = -\frac{\Lambda d}{l_d l_b} \, . \tag{5.13}$$

The lower critical field is estimated in much the same way as Abrikosov calculated H_{c1} for a superconductor. In the smectic phase the elastic free energy depending only on the layer displacement field u and variations in the director field $\delta\hat{n}$ is

$$F_{el} = \frac{1}{2} \int d^3x \left\{ B(\nabla u - \delta\hat{n})^2 + K(\nabla_\perp \beta)^2 + K_{22}(\nabla_z \beta)^2 \right\} , \tag{5.14}$$

where $\delta\hat{n} = (\cos\beta - 1, \sin\beta, 0)$ and $B = C|\psi|^2 q_A^2 = C|r|q_A^2/g$. The elastic energy cost for introducing screw dislocations is calculated by assuming $l_d, l_b \longrightarrow \infty$. The above expression for F_{el} can then be linearised about $\beta = 0$ so that $\delta\hat{n} \simeq \beta\hat{x}$. Minimisation of F_{el} with respect to u and β gives

$$\frac{\delta F_{el}}{\delta u} = -B\nabla \cdot (\nabla u - \delta\hat{n}) , \tag{5.15}$$

and*

$$\frac{\delta F_{el}}{\delta \beta} = -(K\nabla_\perp^2 + K_{22}\nabla_z^2)\beta - B(\nabla_y u - \beta) . \tag{5.16}$$

Knowing that the integral of Vu around a closed contour enclosing a dislocation is nd and using Eqs. 5.15 and 5.16, Renn and Lubensky have shown that the energy per unit length of a screw dislocation is

$$\epsilon = \frac{Bd^2}{2\pi} \ln\left(\frac{\lambda_2}{\xi}\right) + \epsilon_{core} \ . \tag{5.17}$$

Neglecting interactions between screw dislocations and using Eq. 5.12 for $\langle q_{tgb} \rangle$, the free energy density close to the lower critical chiral strength Λ_{c1} is

$$\mathbf{F} = \frac{1}{l_d l_b}(\epsilon - \mathrm{Ad})) \ . \tag{5.18}$$

The threshold chirality at which the energy gained by introducing twist becomes greater than the energy cost for creating dislocations is

$$\Lambda_{c1} = \epsilon/d \ . \tag{5.19}$$

The last two expressions are valid only for $\lambda_2/\xi \gg 1$.

The determination of the upper critical field is much more complicated. In Ref.[8], it is obtained as

$$\Lambda_{c2} = \sqrt{2}\kappa_2 \Lambda_c \ . \tag{5.20}$$

The TGB_A state is stable for $\kappa_2 > 1/\sqrt{2}$.

Renn and Lubensky also investigated the stability of the TGB structure near the point where the nematic, smectic-A and smectic-C phases meet (NAC point) when the chirality is increased from zero [62]. The basis for the calculation was the Chen-Lubensky (CL) model extended to include molecular chirality. The phase diagram obtained using this model is shown in Fig. 5.4. The structure of the TGB_C phase predicted by them is shown in Fig. 5.5a. A TGB_C phase was later discovered by the Bordeaux group [57, 44]. The observed structure was different from that predicted by theory in that the smectic layers were tilted with respect to the grain boundaries (Fig. 5.5b).
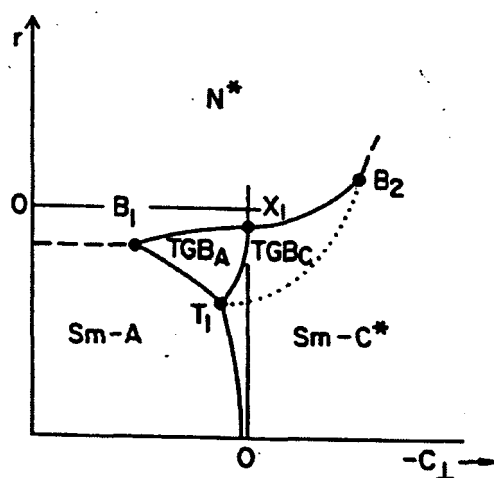
Figure 5.4: The phase diagram obtained by Renn and Lubensky using an extended CL model (after Ref. [62]).
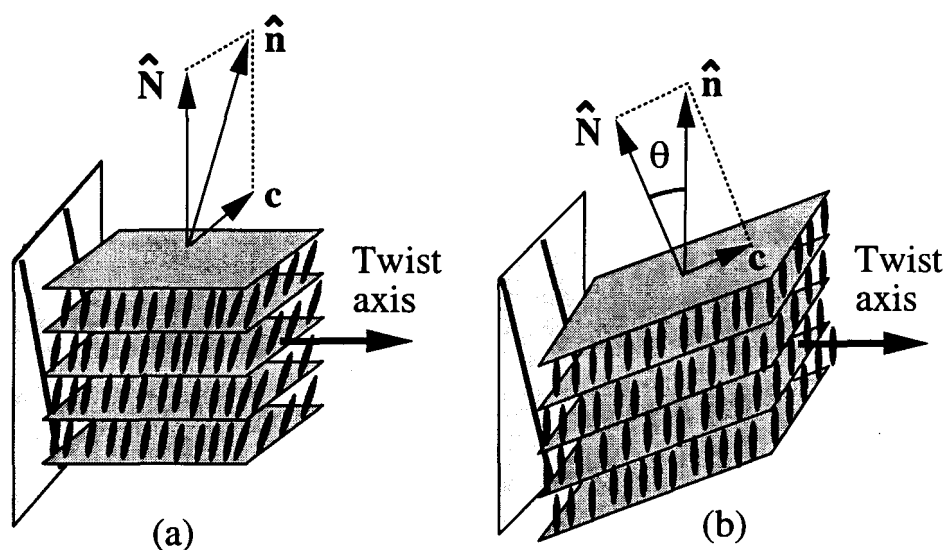

Figure 5.5: A schematic diagram of (a) the theoretically predicted TGB_C structure. The grain boundaries are orthogonal to the smectic layering. The molecules are tilted with respect to the layer normal. The tilt direction is parallel to the grain boundaries (N-c plane is parallel to the grain boundaries). (b) The TGB_C structure observed by the Bordeaux group. In this the smectic layers themselves are tilted with respect to the grain boundaries. In both cases, the twist deformation occurs along the grain boundary normal and the director is everywhere orthogonal to the twist axis (N-c plane is perpendicular o the grain boundaries).

The TGB states are much more complicated than the Abrikosov state in superconductors. This is because in liquid crystals the various physical properties are highly anisotropic. Moreover, since the arrays of screw dislocations in adjacent grain boundaries are at an angle with respect to each other, the interaction is not isotropic as in the case of the parallel set of flux tubes in the Abrikosov phase. This makes the estimation of the two important lengths, l_d and l_b, difficult even in the case of the TGB_A structure. The full elastic free energy expression is quite complicated even in the case of smectic-A. For example, there is no analogue of the $(\mathbf{V}.\hat{n})$ distortion in the case of superconductors. In the analysis of the TGB_A structure, the elastic free energy expression was simplified by Renn and Lubensky. The complexity increases considerably when the symmetry of the layers is lowered from that of smectic-A to that of smectic-C*. There is still no detailed theory explaining the stability of the experimentally observed TGB_C phase, which has a different structure from that predicted by theory. In the observed TGB_C structure, the smectic layering is at an angle with respect to the grain boundaries as represented in Fig. 5.5b. Therefore, the dislocations, which are now at an angle with respect to the layers, are no longer pure screw dislocations. This, plus the fact that now there is also a tilt order make any detailed analysis difficult.

By making a highly simplified analysis, Dozov has argued that if the smectic tilt angle is non-zero, a melted grain boundary is favoured over one with an array of screw dislocations [63]. According to this model the smectic order vanishes over the entire plane of the grain boundary. The minimum energy configuration has the smectic layers tilted with respect to the grain boundaries as seen experimentally.

The situation is far worse in the case of the $UTGB_{C^*}$ phase. Here the grain boundaries have a modulated structure. Furthermore, the structure within the blocks is very complex and is not fully understood. In the proposed structure for this phase, the director configuration with respect to the layering varies from block
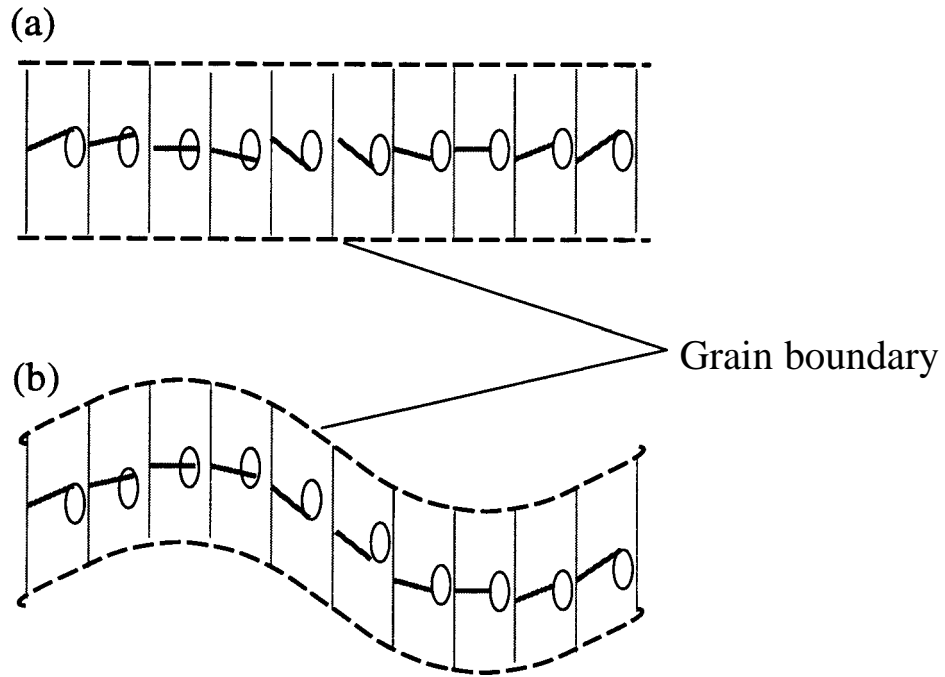
Figure 5.6: A schematic representation of (a) a smectic-C* block with parallel interfaces and (b) a smectic-C* block with undulating interfaces. In the former case the director makes various angles with the interface whereas in the latter case the director is everywhere parallel to the local tangent to the interface.

to block. We have attempted a highly simplified analysis in order to gain some insight into the thermodynamic stability of the various observed TGB phases.

5.2   A simple model for the TGB structures

In this analysis, we treat the grain boundaries as interfaces with an anisotropic interfacial energy. The free energy of the $UTGB_{C^*}$ structure is calculated by assuming an ansatz for the director field within the blocks. The experimental observations show that in this phase, within the blocks, the director has a helical arrangement which is reminiscent of the smectic-C* structure. Also, the grain boundaries have a two dimensional height modulation. A possible physical origin of the undulatory nature of the grain boundaries is discussed below.

5.2.1 Why do the grain boundaries undulate?

Chiral interactions favour a twist deformation in the Frank-director. This tendency is expressed by the term linear in ($\mathbf{ii} \cdot \nabla \times \mathbf{ii}$) in the Frank free energy expression (Eq. **5.2**). The director distortion is a pure twist if the director is confined to a set of parallel planes orthogonal to the twist axis, like in the cholesteric (Sec. **1.1.2**). This is the case in TGB_A and TGB_C structures, where planes containing the director are always parallel to the grain boundaries and the twist deformation is along the orthogonal direction. However, if the director configuration is like that of smectic-C*, then a flat grain boundary is not the best way of maximising the twist deformation across it. For simplicity, let us assume that a single smectic-C* block is boundsd by grain boundaries on both sides. If the grain boundaries are flat the molecular tilt directions in different smectic layers make varying angles with respect to the grain boundaries as shown in Fig. **5.6a**. This means that the distortion across the grain boundaries can no longer have the character of a pure twist. On the other hand, if the grain boundaries are allowed to undulate with the same periodicity as the smectic-C* structure, the director can be made to become parallel to the local tangent to the grain boundary at all points. This situation is schematically shown in Fig. **5.6b**. This increases the value of ($\hat{\mathbf{n}} \cdot \nabla \times \mathbf{ii}$) in the grain boundary region at the expense of other deformations, thus increasing the gain in chiral energy. The actual situation, however, is much more complicated than this simplified picture. Experimental observations suggest that the grain boundaries have a *two-dimensional* modulation with mutually orthogonal wave-vectors. Also, all the grain boundaries undulate along the same two directions. But the smectic layer normal rotates from block to block. Therefore, the director configuration can be expected to be different in different blocks. A simple analysis where the grain boundaries are assumed to be interfaces with an anisotropic interfacial energy shows that the grain boundary energy is lower for an undulating grain boundary compared to that of a

flat one.

In our calculations, we model the grain boundary and the smectic blocks as described in the following sections.

5.2.2   Modelling the grain boundaries

In the TGB_A and the TGB_C phases the grain boundaries are flat and are orthogonal to the TGB twist axis. The Frank-director has a pure twist deformation across each grain boundary. The twist deformation decays exponentially on going away from the grain boundary [6]. Thus, the grain boundary region is highly distorted compared to the smectic blocks. Therefore, we treat the grain boundaries as interfacial regions separating adjacent smectic blocks. If l_d is the separation between screw dislocations within a TGB_A grain boundary and ϵ the energy per unit length of the dislocation, given by **Eq.** 5.17, the dislocation energy per unit area of the interface can be estimated to be (see Sec. 5.1.1)

$$\gamma \simeq \frac{\epsilon}{l_d} \, .$$
(5.21)

γ can be treated as an interfacial tension.

In the case of the $UTGB_{C*}$ phase the interface develops undulations along two mutually orthogonal directions. This can be expected to cost additional energy mainly due to an increase in the length of each screw dislocation. These effects are phenomenologically taken into account by the interfacial tension γ. Experiments show that all the grain boundaries undulate along the same two directions. If the TGB twist axis is taken to be along the Z-axis, the undulation can be described by a height function $h(x, y)$. The simplest form of h which gives a two-dimensional modulation of period $2\pi/q_u$ is

$$h(x,y) = A \, \cos(q_u x) + A \, \cos(q_u y) \, .$$
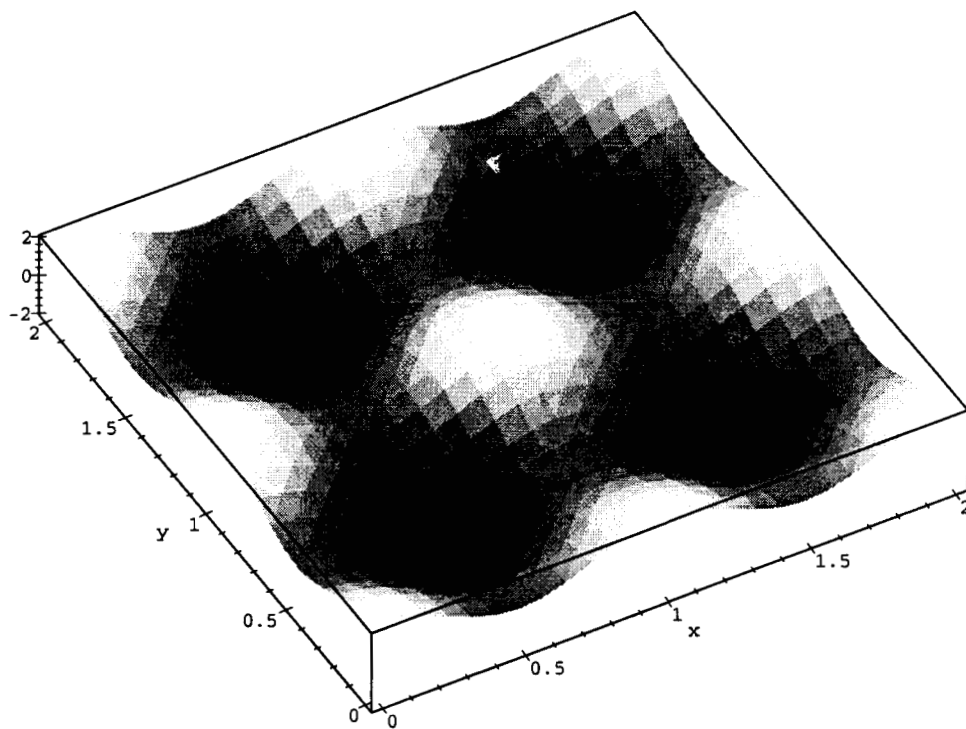(5.22)

This height modulation is plotted in Fig. 5.7.

Figure **5.7:** A plot of the height function Eq. 5.22 describing the two-dimensional modulation of the grain boundaries.

The interfacial energy has a part which is simply proportional to the surface area. If y is the 'interfacial tension', this energy per unit projected area on the XY-plane is given by

$$f_{int} = \gamma\sqrt{(\nabla_x h)^2 + (\nabla_y h)^2 + 1} \; . \tag{5.23}$$

As mentioned in the previous section, the director prefers to be parallel to the interface so that the director distortion across the interface is mainly of twist type. Any deviation from this preferred orientation can be expected to cost a positive energy. This is analogous to the anisotropic interfacial tension at a SmA-isotropic or SmC-isotropic interface (see **Sec.** 2.1.2) [64, 65]. This anisotropic energy cost can be expressed as

$$f_{aniso} = \Delta\gamma(\hat{\mathbf{n}} \cdot \hat{\mathbf{l}})^2 \; , \tag{5.24}$$

where $\hat{\mathbf{l}}$ is the unit normal to the interface and Ay > 0. For small amplitude undulations, the normal to the interface can be expressed as

$$\hat{\mathbf{l}} = \frac{(-\nabla_x h, \; -\nabla_y h, \; 1)}{\sqrt{(\nabla_x h)^2 + (\nabla_y h)^2 + 1}} \tag{5.25}$$

With $\hat{\mathbf{n}} \equiv (n_x, \; n_, \; n_,)$,

$$(\hat{\mathbf{n}} \cdot \hat{\mathbf{l}})^2 = \frac{(-n_x \nabla_x h - n_y \nabla_y h + n_z)^2}{(\nabla_x h)^2 + (\nabla_y h)^2 + 1} \tag{5.26}$$

There is a twist deformation associated with each interface. Most of this deformation is confined to the interfacial region. Introducing interfaces is favourable when the chiral energy gained due to this twist across the interface exceeds the positive contribution given by $f_{int} + f_{aniso}$. In the TGB_A phase, the average rate of twist is given by

$$\langle q_{tgb} \rangle = \langle (\hat{\mathbf{n}} \cdot \nabla \times \hat{\mathbf{n}}) \rangle \simeq \frac{\Delta\beta}{l_b} \; , \tag{5.27}$$

where $\Delta\beta$ is the relative angle between the smectic layer normals of any two adjacent blocks (**Eq.** 5.12). This twist across each interface gives an average gain in the chiral

energy per unit volume (see Eq. **5.2**)

$$f_{twist} = -\Lambda \langle q_{tgb} \rangle = -\Lambda \frac{\Delta \beta}{l_b} \ .$$ (5.28)

As shown in Fig. 4.17 in **Sec.** 4.2.6, the pitch of the TGB structures as well as that of the cholesteric increases as the temperature is reduced. The increase becomes quite sharp in the TGB_C and the $UTGB_{C^*}$ phases. However, for the sake of simplicity, we will assume that $\Delta \beta$ and l_b remain constant in all the TGB phases for a given chiral strength A. ie., we neglect changes in the TGB pitch with temperature. The twist energy gained across the interface also can be expected to vary when the interface becomes modulated. We assume that any reduction in the twist energy due to the modulation is included in the positive contributions from f_{int} and f_{aniso}.

5.2.3 Modelling the blocks

In the TGB_A phase the blocks have a smectic-A-like order. Below a certain temperature, the director in the blocks starts to develop a tilt with respect to the local layer normal. This transition can be described by a simple phenomenological Landau type model developed for describing the smectic-A to smectic-C* transition [66].

The smectic-A to smectic-C* transition is usually second-order in nature. The tilt angle increases continuously from zero as the temperature is lowered below the transition point. Since the medium is chiral, the point symmetry of the layers is C_2. This allows the layers to sustain a permanent polarisation along the C_2-axis. It is observed that the temperature at which the tilt becomes non-zero is not very different for the chiral and achiral modifications of otherwise similar compounds. This means that polarisation does not play a crucial role in determining the transition point. Hence the tilt angle θ is usually considered as the primary order parameter and the polarisation **P** is taken as a secondary order parameter. In the smectic-C* phase, the tilt direction varies along the layer normal. An appropriate order param-
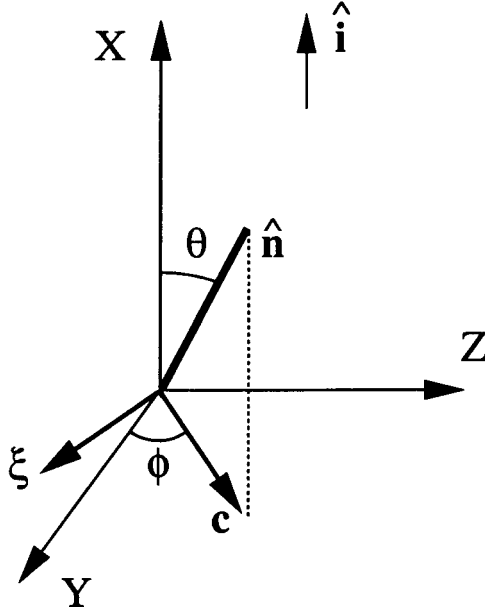
Figure 5.8: The coordinate system used for describing the SmC^* structure. The smectic layer normal, N, is taken to be along the X axis. The vector $\boldsymbol{\xi}$ is orthogonal to c, the projection of $\hat{n}$ on to the YZ plane.

eter which describes the magnitude and the direction of tilt is defined as (Fig. 5.8)

$$\boldsymbol{\xi} = (\hat{n} \times \hat{i}) , \tag{5.29}$$

where the $\hat{i}$ is along the smectic layer normal, N. Thus, $\boldsymbol{\xi}$ is a two-dimensional axial vector and is perpendicular to the c-vector as represented in Fig. 5.8. The components of $\boldsymbol{\xi}$ are

$$\left.\begin{array}{rclcl} \xi_y & = & \sin\theta \sin\phi & \simeq & \theta \sin\phi \\ \xi_z & = & -\sin\theta \cos\phi & \simeq & -\theta \cos\phi \end{array}\right\} , \tag{5.30}$$

where we have assumed θ to be small so that $\sin\theta \simeq \theta$. ϕ is the angle which the c-vector makes with the Y-axis. As already mentioned, the SmC^* phase can sustain a permanent polarisation. In the SmC^* phase, the polarisation-dependent terms will only renormalise some of the elastic constants [66]. Further, in the mixtures we have studied, the polarisation of the pure chiral compound ($CE8$) was extremely small ($4nC/cm^2$) and the addition of an achiral compound is expected to reduce this further. Hence, we ignore all polarisation dependent terms in the following analysis.

The free energy density can then be written as an expansion in $\boldsymbol{\xi}$ and its spatial gradients permitted by the C_2 symmetry. Assuming that there are no distortions in the smectic layering, the invariant combinations can be written as

$$
\begin{aligned}
f \;=\; & \frac{a}{2}\boldsymbol{\xi}^2 + \frac{b}{4}\boldsymbol{\xi}^4 + \frac{K_s}{2}(\nabla \cdot \boldsymbol{\xi})^2 + \frac{K_b^*}{2}(\hat{\mathbf{N}} \cdot \nabla \times \boldsymbol{\xi}) + \frac{K_b}{2}(\hat{\mathbf{N}} \cdot \nabla \times \boldsymbol{\xi})^2 \\
& + \Lambda(\boldsymbol{\xi} \cdot \nabla \times \boldsymbol{\xi}) + \frac{K_t}{2}(\boldsymbol{\xi} \cdot \nabla \times \boldsymbol{\xi})^2 + \frac{K'}{2}(\hat{\mathbf{N}} \times \nabla \times \boldsymbol{\xi})^2 \\
& + \frac{K''}{2}(\boldsymbol{\xi} \times \nabla \times \boldsymbol{\xi})^2 + K_{bt}(\hat{\mathbf{N}} \cdot \nabla \times \boldsymbol{\xi})(\boldsymbol{\xi} \cdot \nabla \times \boldsymbol{\xi}) ,
\end{aligned}
\tag{5.31}
$$

where $a = \alpha(T - T_{AC})$, T being some arbitrary temperature and T_{AC} the temperature below which $\boldsymbol{\xi}$ becomes non-zero. The constant b is positive and is assumed to be independent of temperature. The gradient terms in the free energy density given by **Eq.** 5.31 are basically the same as those used for the SmC in the third chapter, Sec. 3.1.1, except for the chiral terms which are now allowed. However, in Sec. 3.1.1, the free energy expression was written in terms of the c-vector which is orthogonal to $\boldsymbol{\xi}$ and c was taken to be of unit magnitude. The chiral (pseudoscalar) terms in **Eq.** 5.31 are those with the coefficients K_b^* and A. The latter term is usually referred to as the Lifshitz invariant. This term which is permitted by symmetry of the chiral medium produces the helicoidal modulation of the smectic-C* phase.

Before discussing the modelling of the TGB blocks, we first give a brief discussion on the SmC^* striucture.

5.2.3.1 The SmC^* free energy

In order to obtain an expression for the free energy density of the SmC^* phase let us assume that the smectic layers are uniform and the helical distortion is along the X-axis so that $\phi \equiv \phi(x)$ (see Figs. 1.10 and 5.8). Further, we assume the usual one elastic constant approximation, $K_s = K_b = K_t = K^t = K'' \equiv K_c$. Using **Eq.** 5.30 for the components of the vector $\boldsymbol{\xi}$ in the smectic-C* free energy expression, **Eq.** 5.31, and ignoring terms which are of order θ^4 in the elastic part, the free energy density,

Eq. 5.31, reduces to the form

$$f_{C^*} = \frac{a}{2}\theta^2 + \frac{b}{4}\theta^4 + \frac{K_c}{2}\theta^2 \left(\frac{\partial\phi}{\partial x}\right)^2 + \Lambda\theta^2 \left(\frac{\partial\phi}{\partial x}\right) . \tag{5.32}$$

The Euler-Lagrange equation derived from the above expression for a constant θ is

$$\frac{\partial^2\phi}{\partial x^2} = 0 , \tag{5.33}$$

which admits the solution

$$\phi = qx \tag{5.34}$$

Equation 5.32 can then be written as

$$f_{C^*} = \frac{a}{2}\theta^2 + \frac{b}{4}\theta^4 + \frac{K_c}{2}\theta^2 q^2 + \Lambda\theta^2 q \tag{5.35}$$

From Eq. 5.35 it is easy to derive the following thermodynamic properties of the SmC^* phase:

$$q_c = -\frac{\Lambda}{K_c} , \tag{5.36}$$

$$T_{AC}^* = T_{AC} - \frac{1}{\alpha}\left(\frac{\Lambda^2}{K_c}\right) , \tag{5.37}$$

$$\theta_o^2 = \frac{\alpha}{b}(T_{AC}^* - T), \quad T < T_{AC}^* , \tag{5.38}$$

where q_c is the magnitude of the equilibrium wave-vector, T_{AC} the temperature at which the transition would have occurred in the absence of chirality and θ_o the equilibrium tilt angle.

5.2.3.2 Free energy of the TGB blocks

We are mainly interested in the various phases that can occur below the TGB_A phase when the local smectic ordering within the layers changes from SmA-like to SmC-like. Below a certain temperature T_{AC}^*, the smectic layers start developing a tilt order. When this happens, the TGB blocks can be either SmC-like (unwound SmC^*) or SmC^*-like.
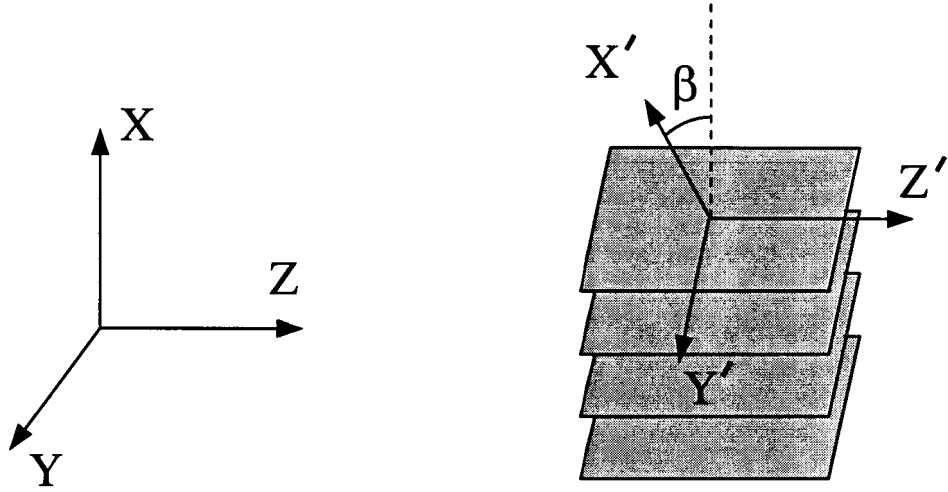
Figure 5.9: Schematic diagram of the coordinate systems used. The (X, Y, Z) system is lab-fixed with the Z-axis along the TGB twist axis. The local (X', Y', Z') system is obtained by a rotation about the Z-axis by an angle β so that the X'-axis is along the local smectic layer normal.

In the TGB_A phase, let the TGB twist axis be along the Z-axis. In the lab-fixed $(X, Y, 2)$-system, the smectic layer normals within the blocks lie in the XY-plane. The smectic layer normal in an arbitrary block makes an angle β with respect to the X-axis. To describe the structure within each block, we choose a local co-ordinate system (X', Y', Z') which is rotated by an angle β about the Z-axis as shown in Fig. 5.9. Thus, the X'-axis is along the smectic layer normal, N, in any given block. Let $\hat{\mathbf{i}}', \hat{\mathbf{j}}'$ and k denote unit vectors along X', Y', and Z', respectively.

The components of the Frank-director in a given block are then given by

$$
\left.
\begin{aligned}
n_{x'} &= \cos\theta \\
n_{y'} &= \sin\theta \cos\phi \\
n_{z'} &= \sin\theta \sin\phi
\end{aligned}
\right\} , \tag{5.39}
$$

where θ is the tilt angle and ϕ is the angle the c-vector makes with respect to the Y'-axis.

In the TGB_A and the TGB_C phases, ξ is assumed to be constant within any given block. In the $UTGB_{C^*}$ phase, however, ξ precesses along the layer normal in each block. Also, since the interfaces have a two-dimensional modulation, ξ can be

expected to be non-uniform within the smectic layers, unlike in the SmC^* phase. Assuming θ to be small, the free energy density of the TGB blocks, given by Eq. 5.31, can be written in the form

$$
\begin{aligned}
f_{block} \;=\; & \frac{a}{2}\theta^2 + \frac{b}{4}\theta^4 + \frac{K_c}{2}\theta^2(\nabla'\phi)^2 + \Lambda\theta^2\frac{\partial\phi}{\partial x'} \\
& -\frac{K_b^*}{2}\theta\left(\sin\phi\frac{\partial\phi}{\partial y'} + \cos\phi\frac{\partial\phi}{\partial z'}\right) \\
& -K_{bt}\theta^3\left(\sin\phi\frac{\partial\phi}{\partial y'} + \cos\phi\frac{\partial\phi}{\partial z'}\right)\frac{\partial\phi}{\partial x'}\,,
\end{aligned}
\tag{5.40}
$$

where the one elastic constant approximation has been applied.

As already explained in Sec. 5.2.2, any deviation of the director from the local tangent plane of the interface costs additional energy. If the director has to be parallel to the interface, the condition

$$
\hat{\mathbf{n}}\cdot\hat{\mathbf{l}} = 0
\tag{5.41}
$$

should be satisfied, where 1 is the normal to the interface. For small amplitude modulations,

$$
1 \equiv (-\nabla_{x'}h',\, -\nabla_{y'}h',\, 1)\,,
\tag{5.42}
$$

where h', obtained by transforming the height function Eq. 5.22 to the local frame, is given by

$$
h'(x',\text{y}) = A\cos\left[q_u(x'\cos\beta - y'\sin\beta)\right] + A\cos\left[q_u(x'\sin\beta + y'\cos\beta)\right]\,.
\tag{5.43}
$$

We first model a block which has its smectic layer normal along one of the lattice-vectors of the square modulation $h'(x',\text{y})$.

Case $\beta = 0$: Using Eqs.5.39 and 5.42 in Eq. 5.41, we get the condition for $\hat{\mathbf{n}}$ to be parallel to the interface as

$$
Aq_u\sin(q_u x') + Aq_u\tan\theta\cos\phi\sin(q_u y') + \tan 6\sin\phi = 0\,.
\tag{5.44}
$$

The above equation (Eq. 5.44) could not be solved analytically. Numerically forcing the director to satisfy the condition given by Eq. 5.44 results in discontinuous jumps

in the +-profile. This is physically unacceptable as the free energy density goes to infinity at the discontinuities. Therefore, we look for director configurations which give a smooth variation of $\phi(x', y')$ within a block and at the same time has a lower value of $\langle (\text{ii}.\, \hat{\textbf{l}})^2 \rangle$ compared to that obtained by having a perfect SmC^* structure within the block. To obtain such a configuration we note that by assuming $Aq_l = \tan\theta$, which is strictly true only for a $1\text{-}D$ modulation as shown in Fig. 5.6, the above equation can be rewritten as

$$\sin\phi + \tan\theta\,\sin(q_u y')\,\cos\phi + \sin(q_u x') = 0 . \qquad (5.45)$$

By inspection of Eq. 5.45, we choose an ansatz for describing the +-distribution in a block with $\beta = 0$ which is of the form

$$\phi(\beta = 0) = -q_u x' - \tan^{-1}\left[\tan\theta\,\sin(q_u y')\right] . \qquad (5.46)$$

This generates a continuous variation of ϕ along the local smectic layer normal, which is parallel to the X'-axis and a periodic distortion within the layers along the Y'-axis.

The director configuration in a block with $\beta = 0$ is schematically represented in Fig. 5.10. Along the layer normal direction, the director precesses about a cone with a period $2\pi/q_u$. Thus, there is a gain in the chiral energy due to the non-vanishing $(\hat{\textbf{n}} \cdot V \times \hat{\textbf{n}})$ contribution. Along the $\hat{\textbf{j}}'$ direction there is an oscillatory behaviour due to the undulation along that direction.

The height function $h'(x', y')$ has a periodicity of $2\pi/q_u$ along the lab-fixed X and Y axes. With respect to the block-fixed frame, this height modulation is periodic along the local smectic layer normal, which is along the X'-axis, only when $\beta = m\pi/4$, where m is an integer. Therefore, we consider only blocks with $\beta = m\pi/4$, for which the periodicity in the director distortions matches that of the height modulation along the local layer normal. With such a large angle between adjacent blocks, the separation between the screw dislocations within a grain boundary is
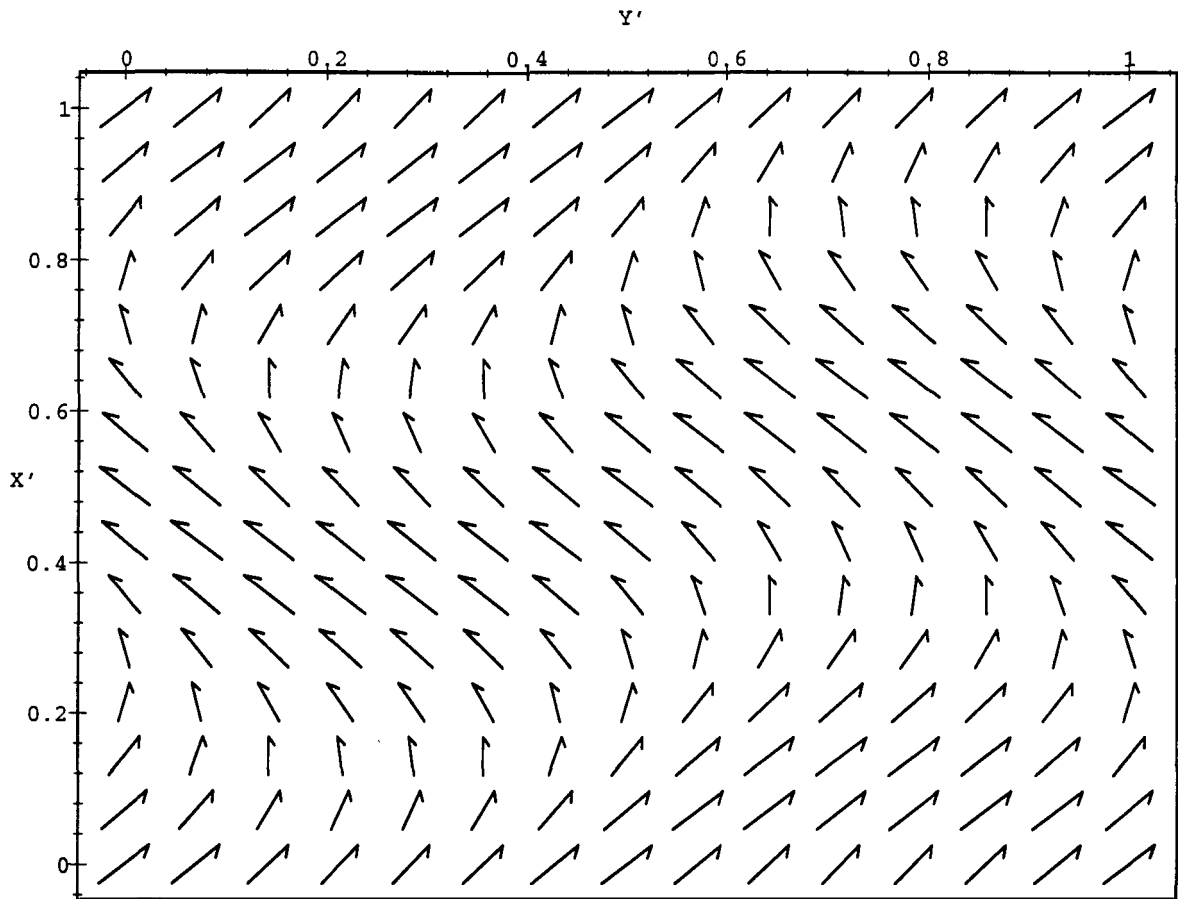
Figure 5.10: A plot of the *projection* of the director field in a block with $\beta = 0$ on to the $X'Y'$-plane. An exaggerated value of $\theta = \pi/4$ was chosen so that the director distortions are easily noticeable. The director precesses along the layer normal which is parallel to the X-axis. Within the layers (along Y-axis) the director has an oscillatory behaviour.
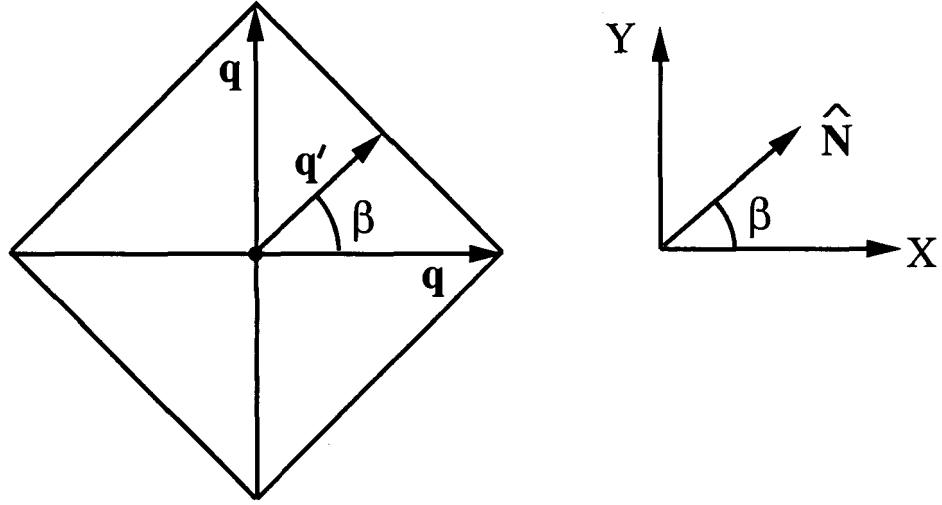
Figure 5.11: The diagram shows how the wave-number of the block structure varies with $\beta = m\pi/4$. Such a variation gives a better matching of the orientation of the director with the interface thereby lowering the interfacial energy.

---

of the order of the layer spacing (see **Eq.** 5.11). This means that the dislocation cores are almost touching each other. In such situations a molten grain boundary description similar to that made by **Dozov** [63] becomes more appropriate and the grain boundaries can indeed be considered as interfaces. Indeed, block-angles as large as 35° have been reported for the TGB_A [67].

The wave-number for director-field in any given block is (see Fig. 5.11)   .

$$q'(\beta = m\pi/4) = q_u/(\sin\beta + \cos\beta) . \qquad (5.47)$$

In analogy with **Eq.** 5.46, the director configuration in an arbitrary block is now assumed to be

$$\phi(x', y') = -q'x' - \tan^{-1}\left[\tan\theta \, \sin(q'y')\right] . \qquad (5.48)$$

For convenience we have replotted the height function corresponding to one lattice spacing along X and Y in Fig. 5.12. The deviations in the director field described by **Eq.** 5.48 from the preferred orientation, over the region shown in Fig. 5.12, for blocks with $\beta = 0$ and $\beta = \pi/4$ are plotted in Figs. 5.13 and 5.14. On the average, the deviations are least for blocks whose layer normals are along one of the lattice
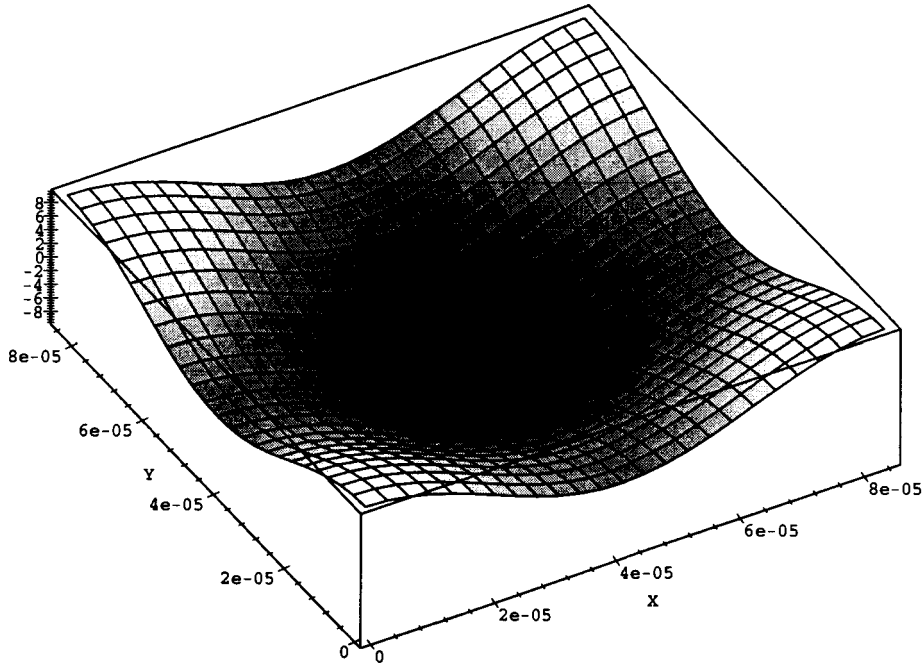
Figure 5.12: The height function, Eq. 5.22, plotted for a lattice spacing, $2\pi/q_u$, along X and Y.

vectors of the square modulation of the interface. The deviations from the preferred orientation costs an energy f_{aniso} given by Eq. 5.24.

We assume that within the blocks ϕ is constant along $\hat{\mathbf{k}}'$, which is the TGB twist-axis direction, since most of the twist distortion is confined to the grain boundary region. In the TGB_A and the TGB_C phases, ϕ is constant along ? and $\hat{\mathbf{j}}'$ also. But in the $UTGB_{C*}$ phase, ϕ varies continuously along $\hat{\mathbf{i}}'$ and oscillates along $\hat{\mathbf{j}}'$. The contribution to the last two terms with coefficients K_b^* and K_{bt} in the free energy expression for the blocks, Eq. 5.40, integrated over a lattice spacing, is equal to zero. Therefore, the free energy density of the blocks can be written in the form

$$f_{block} = \frac{a}{2}\theta^2 + \frac{b}{4}\theta^4 + \frac{K_c}{2}\theta^2\left[\left(\frac{\partial\phi}{\partial x'}\right)^2 + \left(\frac{\partial\phi}{\partial y'}\right)^2\right] + \Lambda\theta^2\frac{\partial\phi}{\partial x'}. \tag{5.49}$$

In the absence of interfaces, the ideal SmC^* structure will have $\phi = q_c x'$ (see Eq. 5.36). Any deviation from this will cost an energy proportional to θ^2 as given by Eq. 5.49.

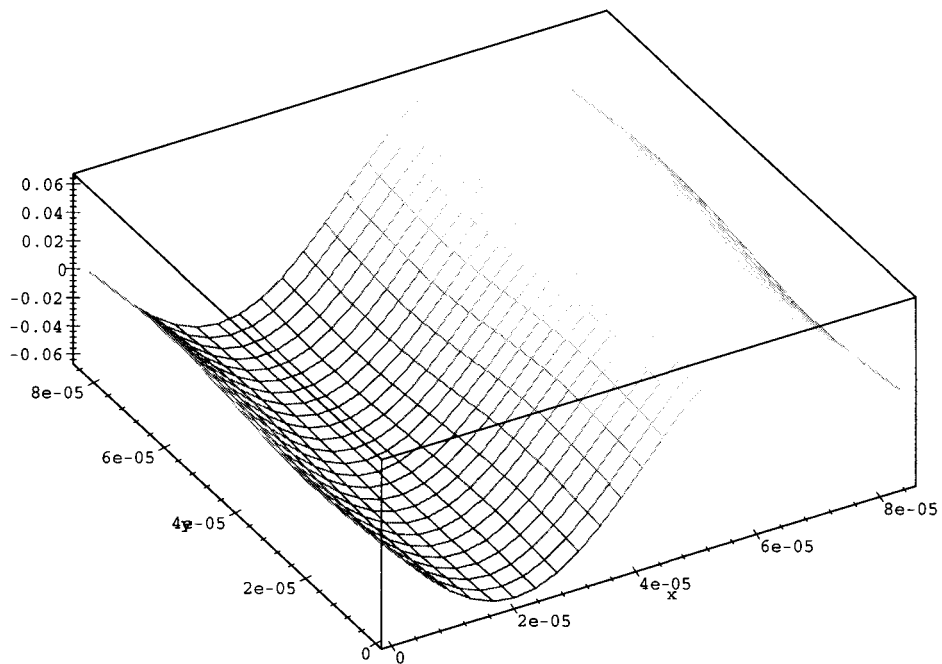In the cholesteric phase, the equilibrium periodicity obtained by minimising the

Figure 5.13: Plot of $\hat{n} \cdot \hat{l}$ over the region shown in Fig. 5.12 for a $UTGB_{C^*}$ block with $\beta = 0$ and $0 = \pi/18$. The optimum value of A and q_t were obtained by minimising the total free energy for the $UTGB_{C^*}$ phase as described later in the text.

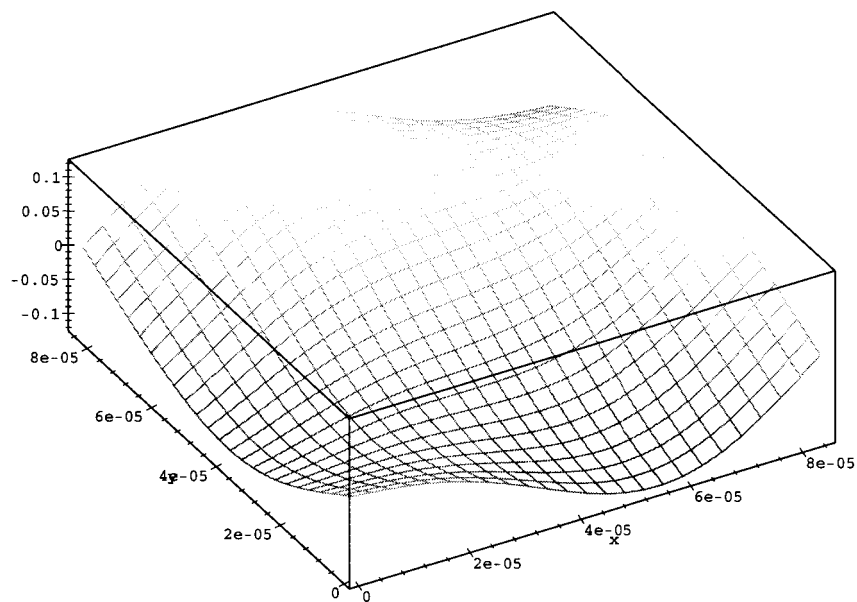Figure 5.14: Plot of $\hat{n} \cdot \hat{l}$ over the same region as shown in Fig. 5.13 with the same values for A and q_t for a $UTGB_{C^*}$ block with $\beta = \pi/4$ and $0 = \pi/18$.

Frank free energy expression is $q_o = \Lambda/K$ (Eq. 5.2). In practice, the pitch of the cholesteric increases as the temperature is lowered. The pitch in the TGB_A phase can be expected to be larger compared to that in the cholesteric phase. Experimentally, we see a more or less continuous increase in the pitch on going from the cholesteric to the TGB_A phase (see, for example, Fig. 4.17). As the temperature is lowered to the $UTGB_{C^*}$ phase, this increase in the pitch becomes very sharp. In our calculations we neglect the temperature dependence of the pitch and we assume the value $\langle q_{tgb} \rangle = q_o/2 = \Lambda/2K$ in the TGB phases.

Since $\Delta\beta = \pi/4$, there are eight blocks in a TGB pitch. This fixes l_b as $l_b = \pi/4\langle q_{tgb}\rangle = \pi K/4\Lambda$.

The free energy density in the various phases are calculated as described below.

5.2.4 Calculations

The various TGB phases and the SmC^* phase can be described as

$$
\left.
\begin{array}{llll}
TGB_A & \Longrightarrow & \theta = 0, & l_b = \pi/4\langle q_{tgb}\rangle, \quad q_u = 0 \\[2mm]
TGB_C & \Longrightarrow & \theta \neq 0, \quad \phi = \text{constant}, & l_b = \pi/4\langle q_{tgb}\rangle, \quad q_u = 0 \\
 & & \quad\quad\quad\text{(in a given block)} \\[2mm]
UTGB_{C^*} & \Longrightarrow & \theta \neq 0, \quad \phi \equiv \phi(x',y'), & l_b = \pi/4\langle q_{tgb}\rangle, \quad q_u \neq 0 \\
 & & \quad\quad\quad\text{(in a given block)} \\[2mm]
SmC^* & \Longrightarrow & \theta \neq 0, \quad \phi = q_c x', & l_b = \infty
\end{array}
\right\}
$$

$$(5.50)$$

where q_u corresponds to the periodicity of the two-dimensional modulation of the interface as described by Eq. 5.22 and q_c to that of the SmC^* helix given by Eq. 5.36.

In the SmC^* phase, with $q_c = -\Lambda/K_c$ (Eq. 5.36), the free energy density given by Eq. 5.32 reduces to

$$
f_{C^*} = \frac{a}{2}\theta^2 + \frac{b}{4}\theta^4 - \frac{\Lambda^2}{2K_c}\theta^2 . \tag{5.51}
$$

In the TGB_A phase, the average energy per unit volume, which is just the sum

of the average interfacial energy f_{int}, and the twist energy, f_{twist}, is

$$f_{TGB_A} = \frac{\gamma}{l_b} - \frac{\Lambda \Delta \beta}{l_b} \; , \tag{5.52}$$

where $\Delta \beta$ is assumed to be $\pi/4$ as in the $UTGB_{C^*}$ phase. There is no contribution coming from f_{block}, since $\theta = 0$.

In the TGB_C phase ϕ is constant in a given block and the only contributions to its free energy density from f_{block} are from the first two terms which are independent of ϕ. This is added to the interfacial part, which is the same as that for the TGB_A to get the average energy density of this phase as

$$f_{TGB_C} = f_{TGB_A} + \frac{a}{2}\theta^2 + \frac{b}{4}\theta^4 \; . \tag{5.53}$$

Unlike in the TGB_A and the TGB_C phases, the block energy in the $UTGB_{C^*}$ phase depends on the orientation of the smectic layer normal with respect to the undulation wave-vectors. Therefore, the total free energy density is averaged over a unit cell. The unit cell is defined by the lattice spacing of the interface modulation $a = 2\pi/q_u$ and the TGB pitch $p_{tgb} = 2\pi/\langle q_{tgb} \rangle$. Using Eqs. 5.23, 5.24, 5.28 & 5.49 for f_{int}, f_{aniso}, f_{twist} and f_{block} respectively, the averaged total free energy density per unit volume becomes

$$\langle f_{UTGB_{C^*}} \rangle = \frac{1}{N} \sum_N \left[\frac{q'^2}{4\pi^2} \int_0^{2\pi/q'} dx' \int_0^{2\pi/q'} dy' \left\{ f_{block} + f_{twist} + \frac{f_{int}}{l_b} + \frac{f_{aniso}}{l_b} \right\} \right] \; , \tag{5.54}$$

where N denotes the number of blocks within a TGB pitch. We choose $\Delta \beta = \pi/4$ so that there are eight blocks in a TGB pitch. It is enough to sum over the first two blocks because blocks which are rotated by $\pi/2$ with respect to each other have the same structure. The averaged energy is then minimised with respect to the undulation amplitude A and the wave-vector magnitude q_u. The integration was performed by the Gaussian Quadrature method [39] and the two-dimensional minimisation was done using the Simplex method [39].

The constants a and b are fixed such that the temperature variation of theta given by Eq. 5.38 agrees reasonably well with the experimental data shown in Fig. 4.22. We choose a value for K which is typical of the cholesteric phase. For simplicity, we take $K_c = K$. A rough estimate of the grain boundary energy for the TGB_A phase near the lower critical chiral strength can be obtained as follows. From **Eq.** 5.19, $\epsilon = \Lambda_{c1}d$. The energy per unit area of the grain boundary is y $\simeq \epsilon/l_d$. With the values (in CGS units) $\Lambda_{c1} = 0.04$, $d = 30$ x 10^{-8} and $l_d = 100$ x 10^{-8} we get y $= 1.2$ x 10^{-2}. Note that this is of the same order of magnitude as the interfacial tension estimated for for the smectic-isotropic interface $(\sim 10^{-2} dyn/cm)$ [64]. The anisotropic tension for the smectic-isotropic interface is expected to be about 1.5 times larger [64].

Based on the above considerations, the following parameters were chosen for the calculations (in cgs units): $a = 0.1$ and b $= 50.0$, $K_c = K = 0.2 \times 10^{-6}$, $\gamma = 3.0$ x 10^{-2}, and $T_{AC}^* = 63.0^oC$.

The average free energy densities in the various phases were calculated as functions of temperature for different values of A and Ay. The results of these calculations are discussed in the next section.

5.2.5   Results and discussion

Figure 5.15 shows the phase diagram obtained as a function of Ay, which is the anisotropic part of the interfacial tension. The temperature vs chiral strength phase diagram is shown in Fig. 5.16. The variations in the lattice spacing and amplitude of the square modulation as functions of temperature are shown in Figs. 5.17 and 5.18, respectively.

We are interested in understanding the stability of the various phases that can form below the TGB_A phase. Therefore, we always start with a TGB_A phase above T_{AC}^* and above a critical chiral strength A, $= \sqrt{K\gamma}$, which is obtained from

Eq. 5.52. Below T^*_{AC}, the tilt angle θ becomes non-zero and increases with reduction in temperature according to **Eq.** 5.38. Now the stable phase can be TGB_C, $UTGB_{C^*}$ or SmC^* depending on their relative free energies.

First let us consider the phase diagram constructed as a function of Ay which is shown in Fig. 5.15. For large values of Ay, the TGB_C is preferred as its structure has $f_{aniso} = 0$. As the temperature is lowered, there is a transition from the TGB_C to the SmC^* phase when the chiral energy that can be gained by having a helical structure along the smectic layer normal within each block exceeds the energy gain due to interfaces. Since $f_{aniso} = 0$, this transition is independent of Ay. As Ay is reduced, the additional interfacial energy cost for undulating the interface becomes small compared to the chiral energy that can be gained in the bulk by having a helical structure within the blocks. Hence, a $UTGB_{C^*}$ structure is favoured over that of TGB_C. As 0 increases with decrease in temperature, the interfacial cost increases due to an increase in the undulation amplitude (see Fig. 5.18) and the mismatch of the director at the interface. Also, the energy cost due to the distortion within the smectic layers and that from the deviations in the pitch of the helical structure within the blocks from that of an ideal SmC^* structure given by Eq. 5.36 increases with 0. These factors cause the $UTGB_{C^*}$ phase to go over to a SmC^* phase at lower temperatures. In between there is a narrow range of Ay in which there is a transition from the $UTGB_{C^*}$ to the TGB_C as the temperature is lowered.

The stability regions of the various phases for different chiral strengths shown in Fig. 5.16 are explained as follows:

<u>Low chirality</u>:- When the chiral strength is increased, at some stage (A = A,), the chiral energy gained across an interface becomes slightly larger than the energy cost arising due to the interfacial tension. Above T^*_{AC}, a TGB_A structure is favoured. Below T^*_{AC}, the chiral energy that can be gained by letting the director precess about the layer normal goes as θ^2 (Eq. 5.49). Therefore, when the tilt angle is
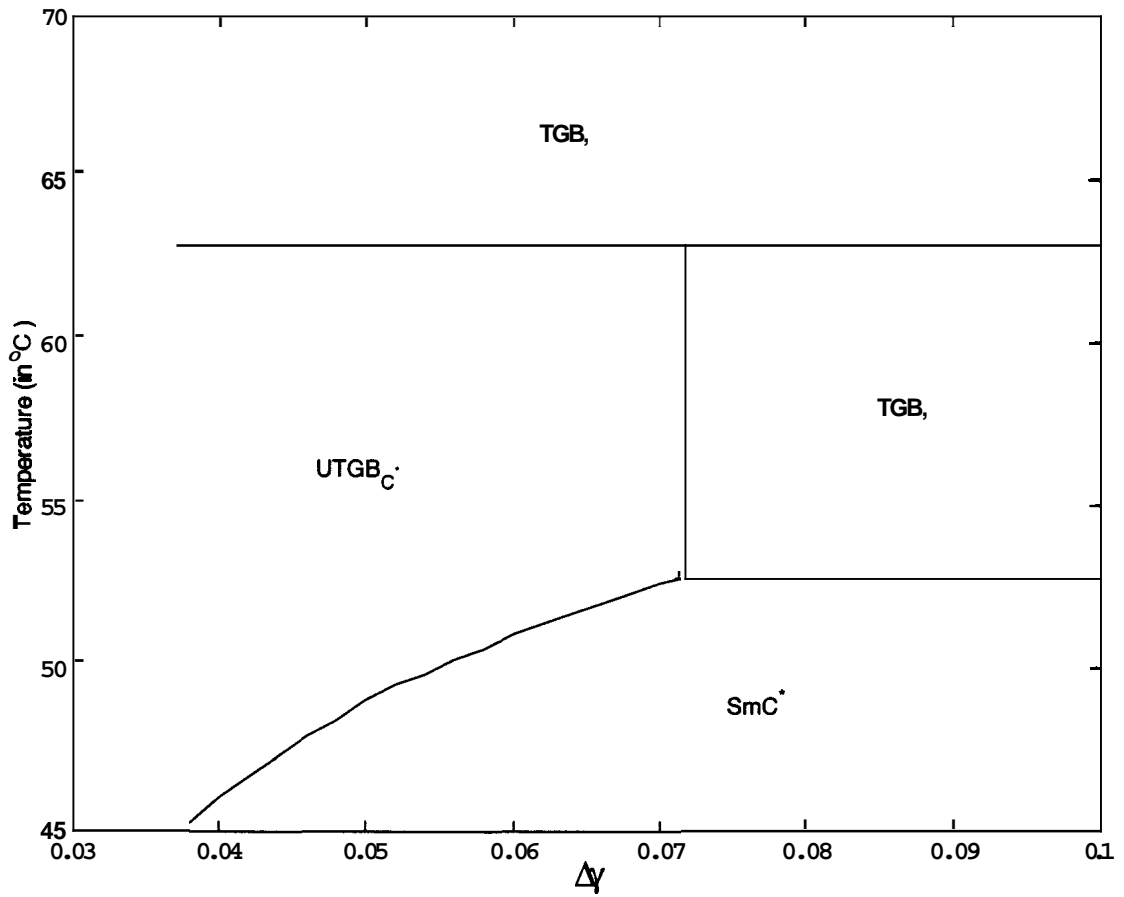
Figure 5.15: The phase diagram showing the stability regions of the various TGB phases and the SmC^* phase as functions of the $\Delta\gamma$ and the temperature T for a given value of $\mathbf{A} = 0.039$. Note that the line separating the $UTGB_{C^*}$ and the TGB_C phases has a finite positive slope.
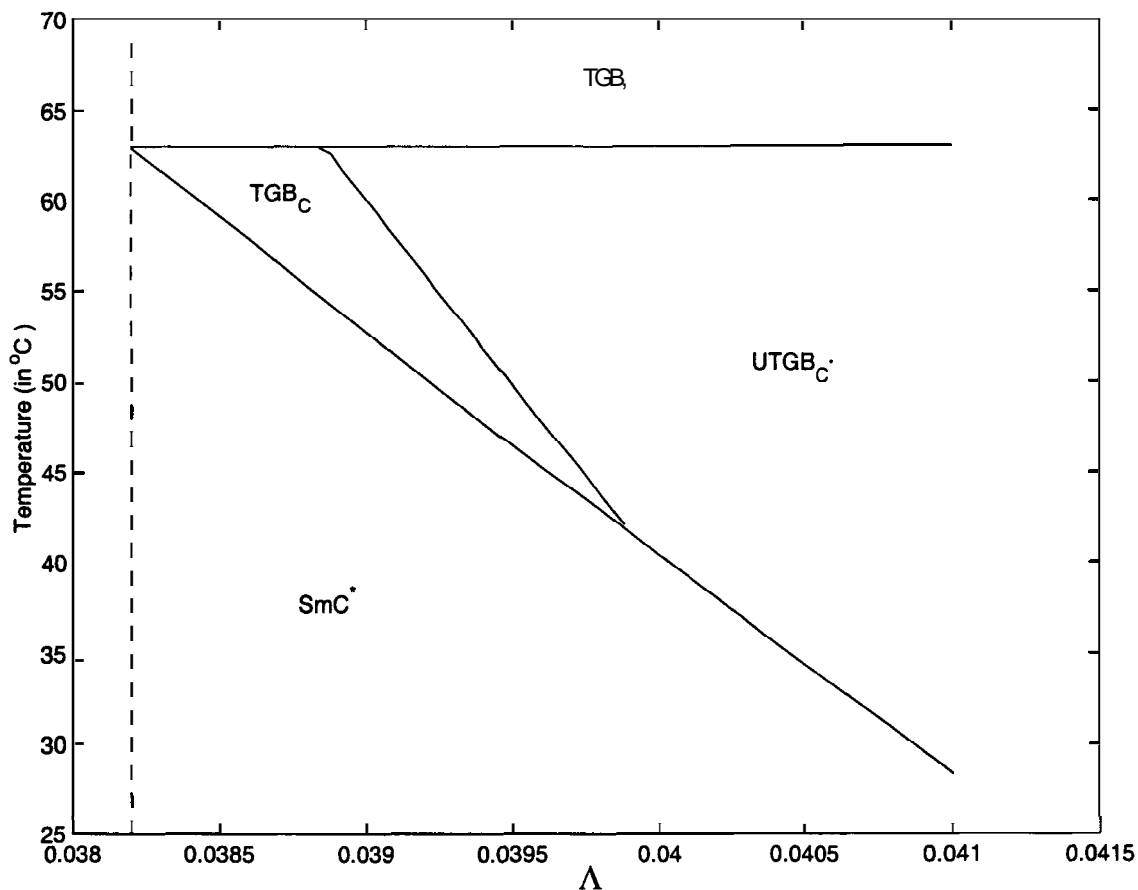
Figure 5.16: The theoretical phase diagram showing the stability regions of the various TGB phases and the SmC^* phase as a function of the chiral strength, $\mathbf{A}$. The value of $\Delta\gamma$ was fixed at 0.072. The vertical dashed line corresponds to the lower critical field $\mathbf{A}, = \sqrt{K\gamma}$ got from **Eq.** 5.52. Below $\mathbf{A}$, the TGB phases are unstable. We are interested only in the phases that occur below the TGB_A phase when the temperature is lowered from $T^*_{AC} = 63.0^\bullet C$ (horizontal line).
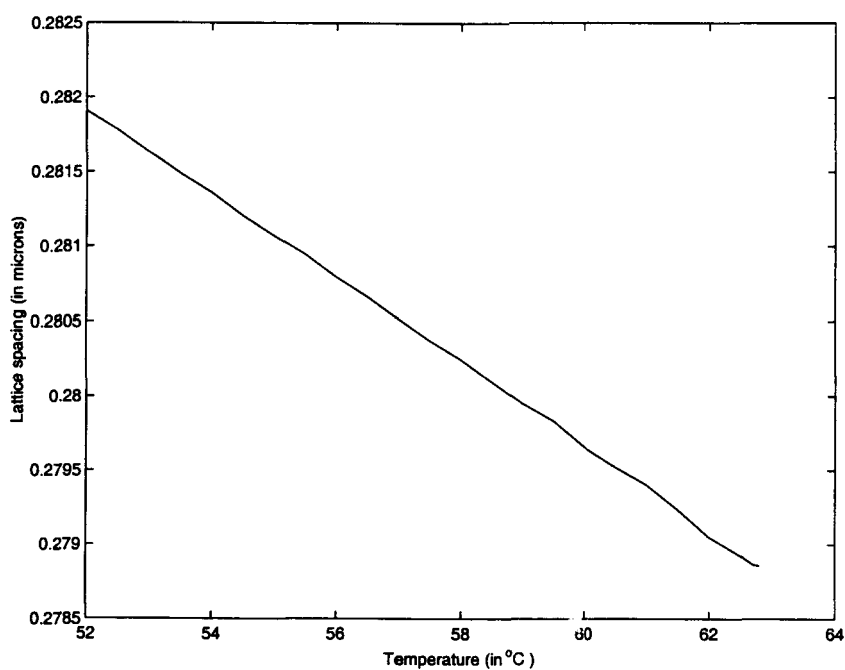
Figure 5.17: Temperature dependence of the lattice spacing $\left(2\pi/q_{u(min)}\right)$ of the square grid, obtained by minimising Eq. 5.54 with respect to A and q_u, as a function of temperature for $A = 0.0396$.
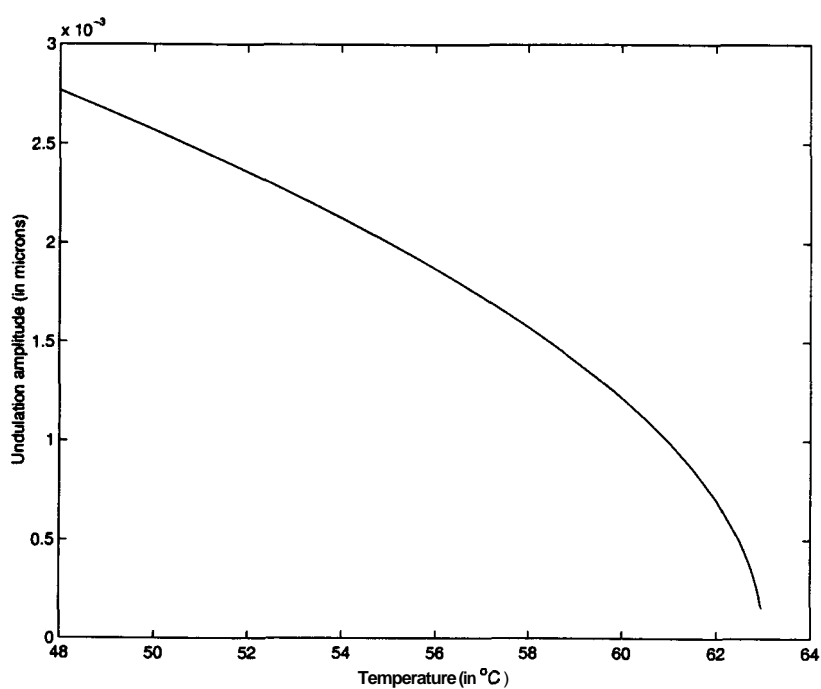

Figure 5.18: Temperature dependence of the amplitude A_{min} of the height modulation as a function of temperature for $A = 0.0396$.

small the chiral energy gained in the bulk by having a helical structure is not very significant compared to the energy f_{twist} gained across a flat interface with $f_{aniso} = 0$. This makes the TGB_C structure more favourable compared to that of SmC^*. The $UTGB_{C^*}$ phase is not preferred because the gain in bulk energy due to a helical structure within the blocks is not large enough to overcome the price to be paid at the interface due to an increase in the surface area, f_{int}, and that due to the mismatch at the interface, f_{aniso}. As the temperature is lowered the chiral energy gain in the bulk increases as θ^2. Below a certain temperature the bulk energy gain in a SmC^* phase exceeds the gain due to the interfaces. The $UTGB_{C^*}$ is still not favoured because f_{int}, f_{aniso} and the positive part of f_{block}, for this structure, also increase with tilt angle and are large compared to the chiral energy that can be gained when the chiral strength is small. Hence there is a direct transition from the TGB_C to the SmC^* phase.

Large chiral strength:- If the chiral strength is large the net energy gain due to an interface becomes large. Hence interfaces are strongly favoured. Also, the energy gain in the bulk by having $UTGB_{C^*}$ blocks becomes considerable even for small tilt angles. But the gain in the bulk free energy due to a helical structure within the blocks alone is less than that from a SmC^* structure. This is due to the distortions within the smectic layers and the deviations in the helical structure in the blocks from that of an ideal SmC^* which cost positive energies. Still this structure is favoured because at high chiral strengths the energy gained in the blocks plus that gained across the interface, f_{twist}, is large enough to overcompensate for the cost due to the additional distortions (compared to an ideal SmC^* structure) within the blocks and that due to $f_{int} + f_{aniso}$. As the temperature is lowered, the positive contribution to the interfacial energy, $f_{int} + f_{aniso}$, increases both due to an increase in surface area and that in the mismatch at the interface with the increase in the tilt angle. Also, the difference between the bulk energies of $UTGB_{C^*}$ blocks and

the SmC^* becomes larger. Due to these two reasons, there is a transition from the $UTGB_{C^*}$ to the SmC^* phase below a certain temperature.

5.3 Conclusion

In conclusion, we have carried out a simple minded analysis of the stabilities of the various TGB phases. In this, the grain boundaries are treated as uniform interfaces. The blocks and the grain boundaries in the $UTGB_{C^*}$ phase were modelled using an ansatz based on the experimental studies described in the previous chapter. Although many details of the structure of the blocks and the grain boundaries are not included, this highly simplified model is able to account for the occurrence of the various TGB phases. The detailed phase diagram will depend on the temperature variation of the various parameters. The values of y and Ay as well as the elastic constants can be expected to increase as the temperature is reduced. This could be one of the reasons for the experimentally observed increase in the TGB pitch with reduction in temperature. In the above analysis, the temperature dependences of these parameters were ignored. However, we believe that this simple model captures some of the physical mechanisms responsible for the formation of these highly complex structures.